ISBN: 978-981-18-5852-9
WCSE 2022 Spring Event: 2022 9th International Conference on Industrial Engineering and Applications
doi: 10.18178/wcse.2022.04.131

Model Predictive Control with Variable Virtual Voltage Vectors for Isolated Matrix Rectifier

Wenlang Deng [1], Zhenjia Geng [2] ,Wei Huang[3], Chun Wang[4]

College of Automation and Electronic Information,Xiangtan University

Abstract. This paper introduces a novel model predictive control (MPC) method with the variable virtual voltage vectors (VVs) applied to the isolated matrix rectifier (IMR) in the power conversion system. This control method solves the problem that the switching frequency is not fixed in the conventional MPC and improves the dynamic response capability and robustness. The IMR is simplified by the idea of decoupling, which realizes the flexible and independent control of its bi-directional switches. Considering the actual industrial production conditions and parameter errors, the position of the virtual VVs can be adjusted. Simulation results verify the effectiveness of the proposed method, showing excellent static and dynamic performance.

Keywords: isolated matrix rectifier, model predictive control, variable virtual voltage vectors, decoupling.

1. Introduction

The isolated matrix rectifier (IMR) evolved from two-stage matrix converter, which inherited many advantages of the latter, such as sinusoidal grid current, high input power factor, compact structure, etc. [1]. The matrix rectifier can introduce a high-frequency transformer to form an isolated matrix rectifier (IMR) so as to achieve electrical isolation and voltage level conversion. At present, IMR has been widely used in fields such as communications, aerospace, V2G, and offshore wind power [2], which has excellent industrial application value.

Model Predictive Control (MPC) was first proposed by American expert Richlet, and it made predictions based on mathematical models and obtained optimal solutions through rolling optimization. The differences between MPC and traditional control methods lie in the state prediction and constraints of the control quantity, so the adverse effects caused by external interference and model mismatch can be eliminated to a certain extent [3]. The control strategy of IMR should adjust the alternating current and the direct current at the same time for realizing the high power factor and the required direct current, but it's not effortless to realize these goals at the same time. Literature [4] uses a widely used proportional-integral (PI) controller to regulate the dc current, but the LC filter produces an inherent phase shift between the grid current and the voltage, resulting in a non-unitary power factor. In order to directly control the power factor, in addition to the dc current control loop, a PI controller is added in [5] to control the phase angle of the grid current. However, the angle is very sensitive to the error caused by the digital sampling process, so it is necessary to design two controllers, which complicates the control strategy. MPC can realize the simultaneous control of multiple control targets. The output current quality index and the size of the reactive power can be reflected in the cost function to constrain, and the cost function can also be modified and expanded according to specific needs. MPC is becoming a more attractive solution for controlling IMR.

MPC is mainly divided into Continuous-control-set MPC (CCS-MPC) and Finite-control-set MPC (FCS-MPC) [6]. FCS-MPC traverses the limited switching state to find the switching state that minimizes the cost function and outputs it directly, without the need for a modulation module, and the algorithm is more concise. FCS-MPC has a large amount of calculation and a long calculation time. In addition, due to the lack of a modulation link, the switching frequency of the switching device is not fixed, and a higher sampling frequency is required to achieve high performance. Literature [7] proposes a pre-selection algorithm based on MPC for matrix converter. First, it calculates the phase angle of the input current vector of the virtual rectifier stage, and then determines the position of the vector in the coordinate system, and finally preselects the nearest vector as the candidate vector for traversal optimization, thereby reducing the calculation amount of

the prediction algorithm. In order to overcome the non-fixed switching frequency of FCS-MPC, the paper [8] proposes to use two vectors in the sector to calculate the cost function of the sector based on the rectifier stage of matrix converter. After traversal optimization, the vector that minimizes the cost function is selected as the action vector at the next moment, and calculates the respective duty cycle. The prediction process of the inverter stage is similar to the rectifier stage, except that a zero vector is additionally introduced, the calculation amount of the entire control scheme is relatively huge.

To sum up, this paper introduces a method of combining both variable virtual voltage vectors (VVs) and basic VVs and applies it to the MPC scheme of IMR. The rest of the paper is organized as follows. In section 2, IMR prediction model is built based on the idea of decoupling. In section 3, the conventional MPC control is introduced. In section 4, the MPC with variable virtual VVs is analyzed in detail. In section 5, we verify the effectiveness of the proposed method through simulation. Finally, we summarize the work of the full paper.

2. Topology and Mathematucal Model of Isolated Matrix Rectifier

2.1. Decoupling and coupling

The IMR topology is shown in Fig.1:

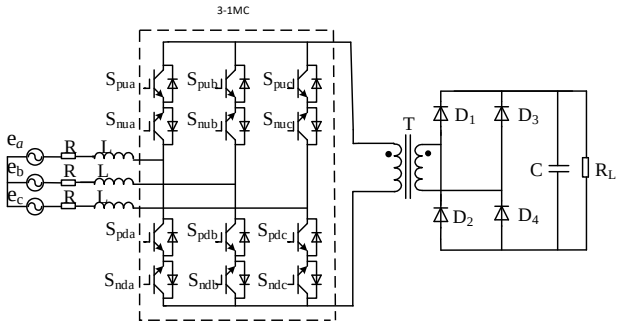

Fig. 1: Isolated matrix rectifier topology.

IMR can be divided into five parts: 1) input filter: voltage-type rectifiers usually only use inductors to filter out the higher harmonics in the grid current, showing a better sinusoidal shape; 2) three-to-single phase matrix converter: output high-frequency electricity with alternating positive and negative; 3) high-frequency transformer: to achieve electrical isolation and voltage conversion between the input side and the output side; 4) uncontrollable rectifier bridge: which changes ac voltage to dc voltage; 5) output filter: the purpose of capacitor is to filter out high-order harmonics of output voltage.

Many papers control the bidirectional switches (S_P and S_n) on the same bridge arm as a whole, i.e. opening and closing together. This article adopts independent control. Switch S_P is used as a normally-on switch, and pulse width modulation (PWM) pulses control the opening and closing of switch S_n. On the contrary, switch S_n can also be used as a normally-on switch, and PWM pulses control the opening and closing of switch S_P. As shown in Fig.2:

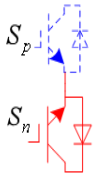

Fig. 2: Switch control mode.

According to the above switch control method, the decoupling of IMR is shown in Fig.3. Decoupling generates positive group converter and negative group converter. When performing space vector modulation (SVM) on the positive group of PWM converter, the switch of negative group is in a normally-on state and outputs positive square wave voltage. When performing SVM on the negative group of PWM converter, the switch of the positive group is in the normal-on state and outputs negative square wave voltage. The bridge circuit in the latter stage rectifies the alternating positive and negative voltage to dc voltage.

The key function of decoupling is to decompose the matrix converter into two groups of ordinary PWM converters, so that the extensive modulation and control strategies applied to PWM converter are suitable for matrix converter.

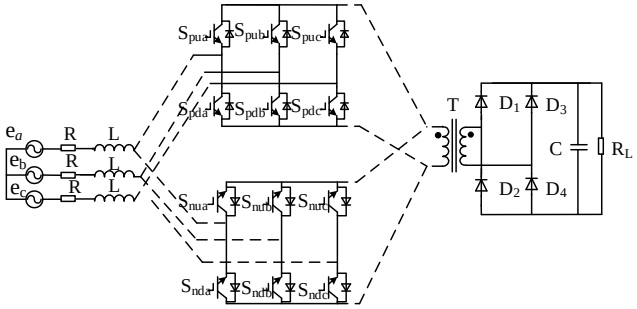

Fig. 3: IMR topology decoupling diagram.

The purpose of coupling is to generate a control signal to the switch tube, and the focus is logical combination. In an "or" gate, the inputs are the drive signal (i=a,b,c) generated by ordinary PWM converter and the coupling control signal (V_P and V_n), and the output is the drive signal of each unidirectional switch after the topology is decoupled. The coupling logic is shown in Fig.4:

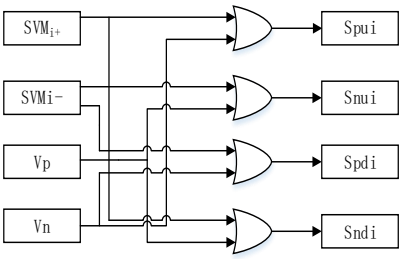

Fig.4: Drive signal coupling logic diagram.

SVM_{i+} and SVM_{i-} are the complementary driving signals of the upper and lower switch tubes of the same bridge arm, and V_P and V_n are complementary high-frequency square waves with a duty cycle of 50% each.

2.2. Build Mathematical Model

According to the above decoupling analysis, taking the positive group rectifier as an example, it outputs positive voltage. In the αβ coordinate system:

$$\begin{cases} u_\alpha = e_\alpha - L\dfrac{di_\alpha}{dt} - i_\alpha R \\ u_\beta = e_\beta - L\dfrac{di_\beta}{dt} - i_\beta R \end{cases} \tag{1}$$

Using Park transformation, the expression in the dq coordinate system is obtained:

$$\begin{cases} u_d = e_d - L\dfrac{di_d}{dt} - i_d R + wLi_q \\ u_q = e_q - L\dfrac{di_q}{dt} - i_q R - wLi_d \end{cases} \tag{2}$$

which is also:

$$u_{dq} = e_{dq} - L\frac{di_{dq}}{dt} - jwLi_{dq} - Ri_{dq} \tag{3}$$

The schematic is shown in Fig.5:

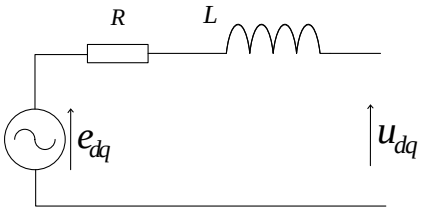

Fig. 5: Equivalent mathematical model.

where: e_{dq} -grid voltage, i_{dq} -grid current, L -filter inductance, w -grid frequency.

According to SVM, the basic VVs are as follows [9]:

$$u_{dq} = \frac{2}{3} U_{dc} e^{j[(n-1)\frac{\pi}{3} - wt]} \qquad \text{n} = [1,2,3,4,5,6] \tag{4}$$

$$u_{dq} = 0 \qquad n = [0,7] \tag{5}$$

The basic VVs is shown in Fig.6:

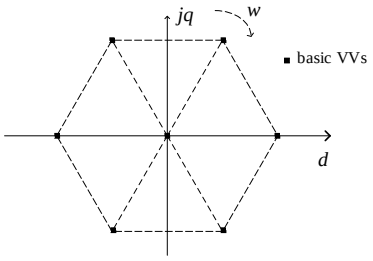

Fig.6: Basic VVs diagram.

The actual voltage vector u_h can be expressed as [10]:

$$u_h = e_{dq} - jwLi_{dq} - Ri_{dq} \tag{6}$$

Combining (3) and (6), we can get:

$$L\frac{di_{dq}}{dt} = u_h - u_{dq} \tag{7}$$

Equation (7) is the basis for predicting the grid current.

3. Conventional Model Predictive Contral

At the current moment, this method predicts the grid current value of the next sampling moment when each basic voltage vector is applied by sampling parameter values, makes a difference with the reference current value, selects the voltage vector that minimizes the difference and applies it to the next sampling moment [11]. The sampling period is T_s. According to the forward Euler formula.

$$\frac{di_{dq}}{dt} \approx \frac{\Delta i_{dq}(k+1)}{T_s} = \frac{i_{dq}(k+1) - i_{dq}(k)}{T_s} \tag{8}$$

Combining (7) to get:

$$i_{dq}(k+1) = i_{dq}(k) + \frac{u_h - u_{dq}}{L} T_s \tag{9}$$

Since the sampling period is very short, it is generally considered that the reference current $i^*_{dq}(k+1)$ at time $k+1$ is equal to the reference current $i^*_{dq}(k)$ at time k, so the difference between the predicted current and the reference current is as follows:

$$\varepsilon_{idq}(k+1) = i^*_{dq}(k) - i_{dq}(k+1) \tag{10}$$

The cost function J of MPC is defined as follows:

$$J = \varepsilon^2_{id}(k+1) + \varepsilon^2_{iq}(k+1) \tag{11}$$

The goal of the MPC algorithm is to select the voltage vector that minimizes the value of J .The overall control scheme is shown in Fig.7:

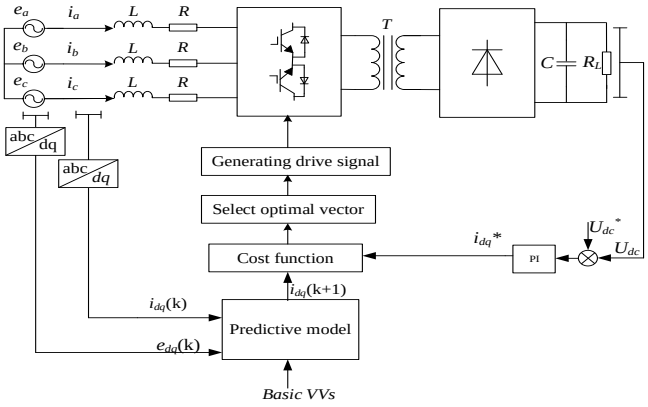

Fig.7: Block diagram of conventional MPC.

4. Model Predictive Contral with Variable Virtual Voltage Vectors

4.1. Control method

In order to further improve the conventional MPC and the MPC with fixed virtual VVs, this paper proposes the MPC with variable virtual VVs. Variation means that the position of the virtual VVs can be changed according to the requirements of the control system. If the system predicts that the optimal output voltage of the rectifier is the reference voltage vector or variable virtual VVs, the SVM module is used to modulate the reference voltage vector or variable virtual VVs to obtain the corresponding switching signal. According to the junction-coupled logic, the switching signal and the complementary high-frequency square wave together perform the control of the two sets of rectifier's switches. Taking one switching cycle as an example, the schematic diagram of each switch driving signal synthesis is shown in Fig.8. SVMa+ and SVMa- represent the complementary driving signal of A-phase generated by modulation, Vp and Vn are voltage switching command signals, Spua and Spda are the driving signals of the A-phase bridge arm of the positive group circuit of the matrix rectifier, Snua and Snda are the driving signals of the A-phase bridge arm of the negative group circuit of the matrix rectifier, and the other two phases are similar to A-phase.

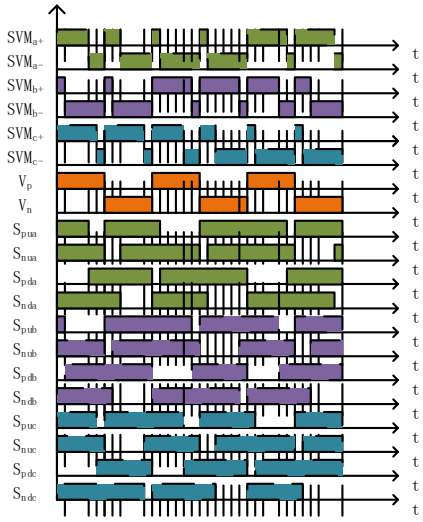

Fig. 8: Schematic diagram of switch driving signals.

The variable virtual VVs are shown in Fig.9. u^*_{dq} is the reference voltage vector that needs to be modulated by the converter based on the goal of the closed-loop control system. The u_1, u_2 and u_3 are variable virtual VVs that located at the three vertices of an equilateral triangle. This equilateral triangle is an inscribed triangle of a circle with u^*_{dq} as the center and R_f as the radius.

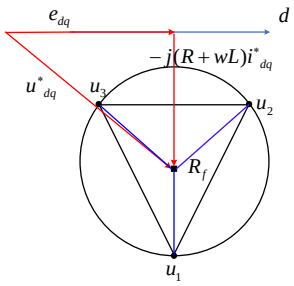

Fig. 9: Schematic diagram of variable virtual VVs.

Therefore, it can be seen that the difference of R_f will lead to different positions of the variable virtual VVs. The choice of R_f will be explained later. In summary, the positions of u_1, u_2, and u_3 can be changed by the u^*_{dq}, so they are called variable virtual VVs. u^*_{dq} is determined by the reference grid current vector i^*_{dq} in the following equation:

$$u^*_{dq} = e_{dq} - j(wL + R)i^*_{dq} \tag{12}$$

The i^*_d is a product of the DC-link voltage controller. Generally, i^*_q is commanded to be 0. The reference voltage vector at time k is :

$$u^*_{dq}(k) = e_{dq}(k) - j(wL + R)i^*_{dq}(k) \tag{13}$$

According to the mathematical characteristics of the equilateral triangle, the variable virtual VVs are obtained:

$$u_1(k) = u^*_{dq}(k) - jR_f \tag{14}$$

$$u_2(k) = u^*_{dq}(k) + j\frac{R_f}{2} + \frac{\sqrt{3}R_f}{2} \tag{15}$$

$$u_3(k) = u^*_{dq}(k) + j\frac{R_f}{2} - \frac{\sqrt{3}R_f}{2} \tag{16}$$

As shown in Fig.10, the variable virtual VVs can be generated from the basic VVs. ‘1’ means that the upper switch of the phase is on, and the lower switch is off, ‘0’ means that the lower switch of the phase is on, and the upper switch is off.

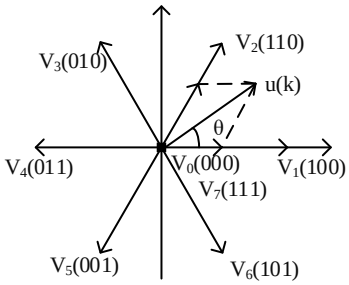

Fig. 10: Synthesis of virtual vectors.

Take the virtual vector between V1 and V2 as an example:

$$u(k) = \frac{T_1}{T_S}V_1 + \frac{T_2}{T_S}V_2 \tag{17}$$

T1 is the action time of V1, T2 is the action time of V2.

$$\begin{cases} T_1 = mT_S \sin(\dfrac{\pi}{3} - \theta) \\ T_2 = mT_S \sin(\theta) \end{cases} \tag{18}$$

where m is Modulation coefficient of SVM:

$$m = \frac{\sqrt{3}}{U_{\mathrm{dc}}} |u(\mathrm{k})| \tag{19}$$

Therefore, the change of grid current is as follows:

$$\Delta i_{dq}(k+1) = \frac{u_h(k) - u_{con}(k)}{L} T_s \tag{20}$$

$$i_{dq}(k+1) = i_{dq}(k) + \frac{u_h - u_{con}}{L} T_s \tag{21}$$

Similar to conventional MPC, the cost function J is defined as:

$$J = \varepsilon^2{}_{id}(k+1) + \varepsilon^2{}_{iq}(k+1) \tag{22}$$

The u_{con} is the voltage vector waiting to be selected and applied to the converter. The following are the specific conditions of selecting: (1) When the inductance parameters are given accurately, that is, the actual inductance value is the same as the nominal value, the system works stably, and the reference voltage vector should be selected to achieve accurate and stable output; (2) In practical engineering applications, the inductance will cause its nominal value to be different from the real value due to aging, that is, there is an error between the inductance value used in the control algorithm and the actual inductance value. The reference voltage vector derived from the mathematical model is different from the actual voltage vector, the prediction algorithm selects the voltage vector that minimizes the cost function value. The control block diagram of the proposed method is shown in Fig.11:

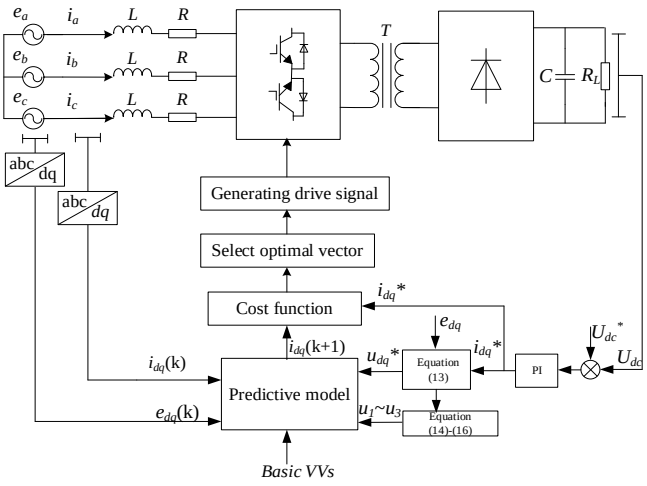

Fig. 11: Block diagram of MPC with variable virtual VVs.

The voltage vectors that can be selected in the system include 16 basic VVs of the positive group and negative group converters, reference voltage vector, and 3 virtual voltage vectors, a total of 20 voltage vectors. The control flow of the system is shown in Fig.12.

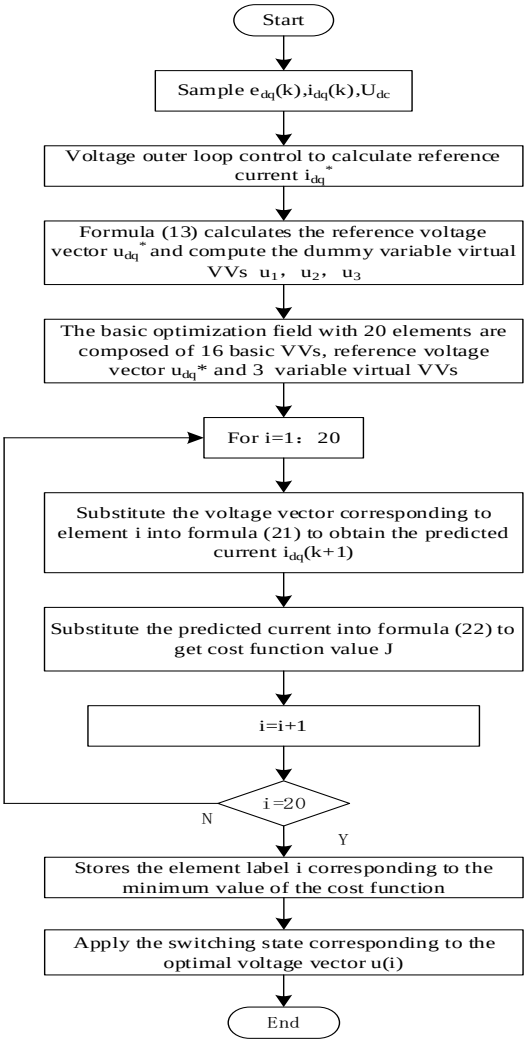

Fig. 12: Control flow diagram.

Based on the above control scheme, after the cost function calculation, if the voltage vector applied to the converter is u^*_{dq} or u_1, u_2, u_3, space vector modulation is required. The two groups of converters perform modulation work alternately, so that the high-frequency transformer outputs positive and negative high-frequency square wave signals, and then the output of dc voltage is realized by the uncontrolled rectifier bridge circuit of the latter stage.

4.2.Influence of inductance L

The actual value of the inductance in the system is L_{m}, and the actual voltage vector is u_{real} according to formula (6). The inductance value calculated in the model prediction algorithm is the nominal value L, and the reference voltage vector u^*_{dq} derived from the mathematical model by substituting L into equation (13) may no longer be applicable to the system. This strategy provides more voltage vectors for selection, and selects the optimal one to minimize the cost function value. The method for selecting the voltage vector is as follows: (1) When the actual value of the inductance is the same as the nominal value, i.e. $L = L_{\mathrm{m}}$, the reference voltage vector derived from the mathematical model is consistent with the actual voltage vector, so the SVM module can be directly used to modulate the reference voltage vector to obtain the switching signal. (2) Under actual operating conditions, due to factors such as device aging, the nominal value of the inductance often has a certain deviation from the actual value. For this reason, an error threshold is selected in this design to form an equilateral triangle area near the reference voltage vector, as shown in Fig.9. When the actual value of the inductance is slightly larger than the nominal value, for example $L_{\mathrm{m}} = 1.5L$, at this time, it can be seen from the comparison of formula (6) and formula (13) that u^*_{dq} is bigger than u_{real}, that is, u_{real} is located below the reference voltage vector derived from the mathematical model in Fig.9, and will not exceed the triangle area. The system will use the global traversal optimization mechanism to select u^*_{dq} or the nearest

variable virtual VVs as the modulation amount to generate the driving signal. The specific selection method is determined by judging the size of the cost function value of each voltage vector. (3) When the actual value of the inductance is slightly smaller than the nominal value, for example $L_m = 0.5L$, the actual voltage vector is above the u^*_{dq}, and will not exceed the set triangle area. At this time, the system uses the global traversal optimization mechanism to select the u^*_{dq} or the variable virtual VVs on the upper side and generate the drive signal by modulating. (4) When the error between the actual value of the inductance and the nominal value exceeds a larger limit, for example $L_m = 0.25L$, the actual voltage vector is ar above the u^*_{dq}, that is, it exceeds the set triangle area. It can be seen from equation (20) that if u_{con} is u^*_{dq} or variable virtual VVs, the current can only increase. At this time, the range of the voltage vector is selected to include the basic VVs to reduce the cost function value against the change of the curren

The different value of R_f will change the size of the circle and the size of the inscribed triangle, so that the position of the variable virtual VVs will change. Therefor, under the condition that the current is controllable, the size of R_f affects the variation range of the inductance L. In the critical state, the difference between u_h and u^*_{dq} is exactly half of the radius R_f, which is:

$$wL_m i_{dq} - wLi^*_{dq} = 0.5R_f \tag{23}$$

Assuming $i_{dq} = i^*_{dq}$:

$$R_f = 2w\Delta L i^*_{dq} \tag{24}$$

where $\Delta L = L_m - L$,it is the maximum acceptable range of inductance. The value of R_f should be determined and keep unchanged before operating the control system.

5. Simulation

In order to verify the effectiveness of the proposed method, the simulation is implemented in Matlab/ Simulink software. The simulation parameters are shown in Table I:

Table 1: Simulation parameters

Parameters	Value
Grid-voltage e	220V, 50Hz
Filter inductance L	2mH
Input resistance R	0.1Ω
Filter capacitor C	6mF
Load resistance R_L	10Ω
DC-link voltage U^*_{dc}	700V
Sampling frequency	10KHz

In the simulation, we test the output voltage of the system, the phase relationship between grid voltage and current, the harmonic content of grid current and the ability to resist load disturbance. The simulation results are shown in Fig.13:

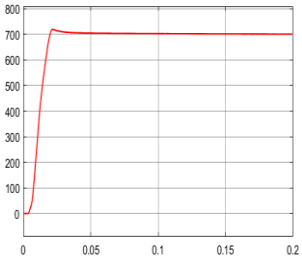

(a) output voltage

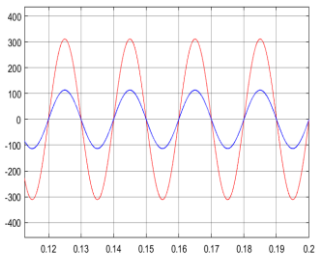

(b) Phase relationship

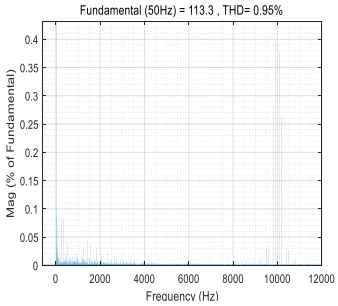

(c) grid current harmonic

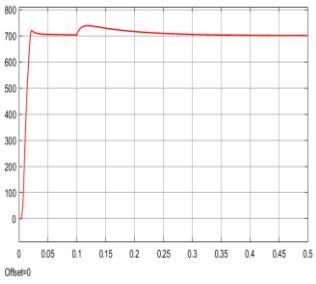

(d) Voltage dynamic recovery

Fig.13: Simulation waveforms.

As shown in Fig.13(a), the output DC voltage of the system is 700V, which is completely consistent with the target voltage value of the closed-loop control system. This result shows that the system can work accurately and stably. In Fig.13(b), the grid current and voltage have the same phase, which means that the power factor of the system can reach 1. It can be seen from Fig.13(c) that the high-frequency harmonic content of the grid-side current is 0.95%, indicating that the system can obtain an ideal quality grid current. At 0.1s, the load resistance suddenly changes from 10Ω to 20Ω. As shown in Fig.13(d), the output DC voltage rises briefly and then returns to its original value, which indicates that the system has a strong ability to resist load disturbance.

When L_m and L are inconsistent, we test the robustness of the proposed method and compare it with conventional MPC. The simulation results are shown in Fig.14 and Fig.15 :

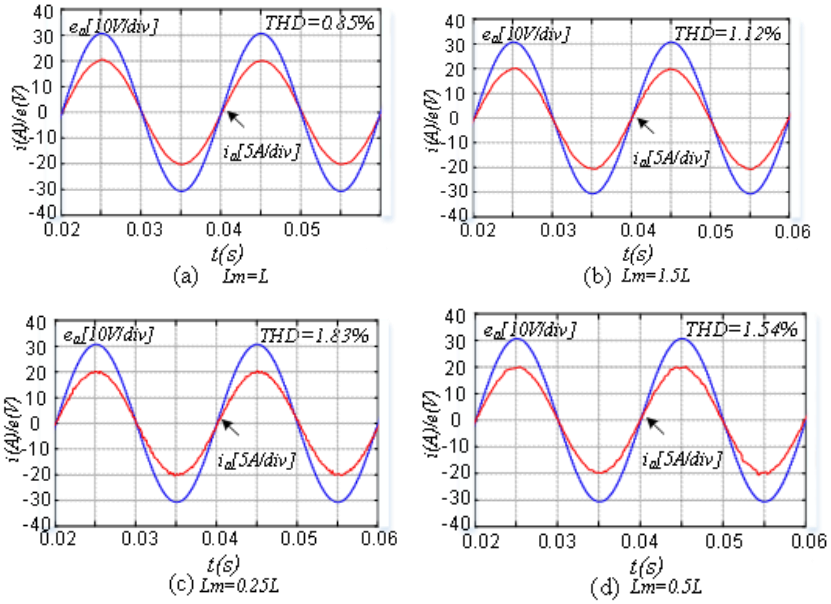

Fig. 14: MPC with variable virtual VVs.

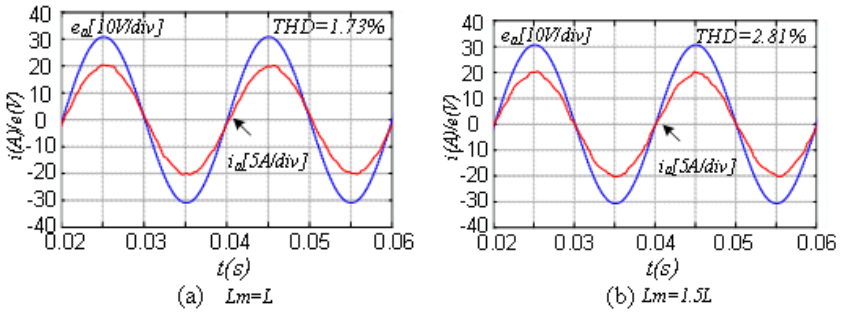

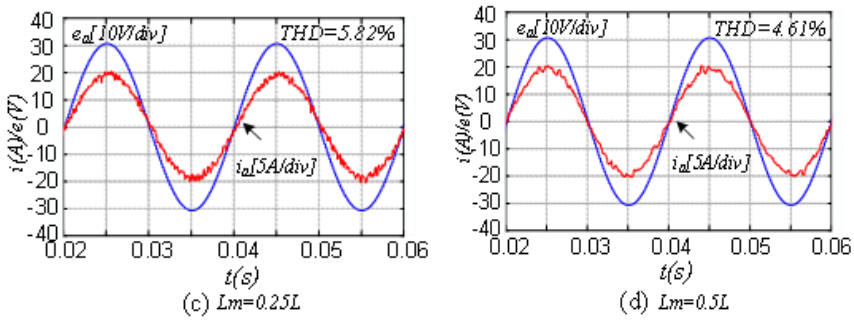

Fig. 15: Conventional MPC.

By measuring the harmonic content of the grid current in the four cases in Fig.14. By measuring the harmonic content of the grid current in the four cases shown in Fig.15. The comparison shows that the proposed control scheme makes the system more robust.

6. Conclusion

This paper combines FCS-MPC with SVM and applies it to the IMR. Compared with the conventional MPC, the proposed method makes the IMR has more excellent static and dynamic output capacity, so it has an eximious industrial application prospect.

7. References

[1] M. Parvez Akter, S. Mekhilef, N. Mei Lin Tan and H. Akagi, "Modified Model Predictive Control of a Bidirectional AC–DC Converter Based on Lyapunov Function for Energy Storage Systems," IEEE Transactions on Industrial Electronics, vol. 63, no. 2, pp. 704-715, Feb. 2016.

[2] Gcr s A, Molinas M, "A Study of Efficiency in a Reduced Matrix Converter for Offshore Wind Farms," IEEE Transactions on Industrial Electronics, 2012, 59(1): 184-193.

[3] Rivera M, Rodriguez J, Espinoza J, "Reduction of Common-Mode Voltage in an Indirect Matrix Converter with Imposed Sinusoidal Input/Output Waveforms," IECON 2012 - 38th Annual Conference on IEEE Industrial Electronics Society. 2012: 6105–6110.

[4] Vargas R, Rodriguez J, Ammann U et al, "Predictive Current Control of an Induction Machine Fed by a Matrix Converter with Reactive Power Control," IEEE Transactions on Industrial Electronics, 2008, 55(12): 4362–4371.

[5] Yan Z, Zhang K, Li J, "A Novel Absolute Value Logic SPWM Control Strategy Based on De-Re-Coupling Idea for High Frequency Link Matrix Rectifier," IEEE Transactions on Industrial Informatics, 2013, 9(9): 1188-1198.

[6] Ahmed A A, Koh B K, Lee Y I, "A Comparison of Finite Control Set and Continuous Control Set Model Predictive Control Schemes for Speed Control of Induction Motors," IEEE Transactions on Industrial Informatics, 2018, 14(4): 1334–1346.

[7] Dan H,Zhu Q,Peng T,et al, "Preselection algorithm based on predictive control for direct matrix converter," IET Electric Power Applications,2017,11(5)：768-775.

[8] Tarisciotti L,Lei J,Formentini A, "Modulated Predictive Control for Indirect Matrix Converter," IEEE Transactions on Industry Applications,2017,53(5)：4644-4654.

[9] Y. Deng and R. G. Harley, "Space-Vector Versus Nearest-Level Pulse Width Modulation for Multilevel Converters," IEEE Transactions on Power Electronics, vol. 30, no. 6, pp. 2962-2974, June 2015.

[10] K. Kulikowski and A. Sikorski, "New DPC Look-Up Table Methods for Three-Level AC/DC Converter," IEEE Transactions on Industrial Electronics, vol. 63, no. 12, pp. 7930-7938, Dec. 2016.

[11] M. Narimani, Bin Wu, V. Yaramasu, Zhongyuan Cheng and N. R. Zargari, "Finite Control-Set Model Predictive Control (FCS-MPC) of Nested Neutral Point-Clamped (NNPC) Converter," IEEE Transactions on Power Electronics.